

# The Pitfalls of Dark Crossings

Stefano Profumo\* and William Shepherd†

*Department of Physics, University of California,  
1156 High St., Santa Cruz, CA 95064, USA and  
Santa Cruz Institute for Particle Physics, Santa Cruz, CA 95064, USA*

Tim M. P. Tait‡

*Department of Physics & Astronomy, University of California, Irvine, CA 92697*

We explore the connection between pair production of dark matter particles at collider experiments and annihilation of dark matter in the early and late universe, with a focus on the correlation between the two time-reversed processes. We consider both a model-independent effective theory framework, where the initial and final states are assumed to not change under time-reversal, and concrete UV-complete models within the framework of supersymmetric extensions to the Standard Model. Even within the effective theory framework (where crossing symmetry is in some sense assumed), we find that the predictions of that symmetry can vary by orders of magnitude depending on the details of the selected effective interaction. Within the supersymmetric models we consider, we find that there is an even wilder variation in the expectations one can derive for collider observables based on cross-symmetric processes such as having a thermal relic or given indirect dark matter detection rates. We also explore additional “pitfalls” where naïve crossing symmetry badly fails, including models with very light mediators leading to Sommerfeld enhancements and/or dark matter bound states.

PACS numbers: 95.35.+d

## I. INTRODUCTION

Understanding the particle nature of dark matter is likely to be a decisive portal towards unveiling the broader picture of physics beyond the Standard Model. Extracting information on dark matter as a fundamental particle relies on the assumption that such particles interact, even if only weakly, with particles in the Standard Model. Processes thus might exist whereby one could obtain more or less direct information about such interactions. The notion that given a process (for example, dark matter elastic scattering off of quarks contained in nuclei) a “conjugated” or cross-symmetric process exists at quantifiable levels (for example, dark matter pair annihilation into quark pairs in the galaxy or quarks annihilating into pairs of dark matter particles at the LHC) is key to the idea of “complementarity” in the search for signatures from dark matter [1].

The key ways in which we can hope to learn about weak-scale weakly-interacting massive particles, commonly known as WIMPs, can be classified in terms of general processes of the following type, where  $\chi$  indicates a WIMP and SM any Standard Model particle:

- *Direct Detection:*  $\chi + \text{SM} \rightarrow \chi + \text{SM}$ ;
- *Indirect Detection:*  $\chi + \chi \rightarrow \text{SM} + \text{SM}$ ;
- *Collider Searches:*  $\text{SM} + \text{SM} \rightarrow \chi + \chi$ .

In addition, processes from the three categories above can lead to other probes of the nature of dark matter (for example elastic scattering sets the temperature for kinetic decoupling of dark matter in the

---

\*Electronic address: profumo@ucsc.edu

†Electronic address: wshepher@ucsc.edu

‡Electronic address: ttait@uci.edu

early universe, which in turn determines the small-scale cutoff to the dark matter power spectrum [2], and the pair annihilation processes determine the thermal relic density of WIMPs from the early universe).

Relating the processes listed above in some quantitative way is an important task, and one that has historically lead to setting important benchmarks for WIMP searches. For example, the assumption that the pair annihilation of WIMPs in the early universe (specifically, at the time of chemical freeze-out) is the same as the annihilation rate in the late universe (for example, in the Milky Way today) produced the expectation for the natural scale of the relevant thermally averaged pair-annihilation cross section times relative velocity  $\langle\sigma v\rangle_0 \simeq 3 \times 10^{-26} \text{ cm}^3/\text{s}$ . This figure, motivated by the requirement of the thermal WIMP relic density from the early Universe matching the observed average dark matter density, is often considered the benchmark for indirect WIMP searches with gamma rays, high-energy neutrinos or antimatter. The weak-interaction level cross section implied by that pair-annihilation cross section also motivates collider studies where, for example, one pair-produces dark matter particles with a cross section at the level implied by the time-reversed process, plus jets or photons [3]. The cross-symmetric  $\chi + \text{SM} \rightarrow \chi + \text{SM}$  process, again with a similarly motivated cross-section level, is employed to set the scale for direct dark matter searches.

Exploring the validity of crossing symmetry arguments to set the stage for making use of complementarity in the search of dark matter is thus a very important task. Clearly, the degree to which crossing symmetry can be used depends on the assumed model for the particle sector comprising the dark matter. In principle, however, it should be possible to use constraints from one class of processes (for example collider searches) to set bounds on or to delineate the relevant parameter space for another class of processes (for example direct detection). This type of exercise has been carried out along several model-dependent avenues, e.g. in the context of supersymmetric dark matter models [see e.g. [4] for a recent study] or in the context of universal extra-dimensional models [e.g. [5]]. Additionally, the possibility that heavy physics described by an effective contact interaction mediates the coupling of the dark matter to Standard Model particles has been widely explored. This has lead to detailed predictions relating direct detection and collider searches for theories featuring higher-dimensional operators representing heavy states that have been integrated out of the effective theory [6–11].

While crossing symmetry is undoubtedly an important theoretical resource to produce predictions for complementary dark matter search channels, it is equally important to appreciate how crossing symmetry arguments might fail. Perhaps the most natural place where crossing symmetry is expected to provide accurate guidance is in the indirect detection versus collider direction, processes that are essentially simply related by time-reversal. In addition, models with the same thermal relic abundance can lead to drastically different outcomes for the directly related indirect detection rates as well as for collider searches.

In the present study, we explore examples of the “pitfalls” of crossing symmetry arguments in the context of dark matter searches. We start with the point that in effective theories, the time-reversal crossing symmetry relating indirect detection (and the relic density) to collider searches can fail drastically, despite the fact that crossing symmetry is, in some sense, assumed by construction (sec. II). We show in sec. III how UV-complete models of dark matter, such as neutralinos in supersymmetric models, can produce widely different outcomes for indirect detection and collider searches even while giving rise to the correct thermal relic abundance, and for the same lightest neutralino mass. Finally, we discuss models where crossing symmetry fails badly, either because the dynamics of the dark sector contains light mediators, leading to richer phenomena than is expected for heavier mediators, or because of the presence of inelastic processes in dark matter scattering (sec. IV). We present our conclusions in sec. V.

## II. MANIFEST CROSSING SYMMETRY FAILING TO MANIFEST

The first class of models we consider is the case in which the particles mediating dark matter’s interactions with the Standard Model are very heavy, leading to a description in terms of contact interactions in the context of an effective field theory (EFT). We work in the simplest constructions where the dark mat-

ter is a SM singlet, and, to be concrete, specialize to the case where it is a fermion<sup>1</sup>. It is straight-forward to generalize our analysis to dark matter of arbitrary spin. We choose the specific EFT implementations of Ref. [6, 8], which consider the lowest-dimension operators with a particular Lorentz structure, keeping the leading terms as dictated by minimal flavor violation [12].

The relation between direct detection and collider signals within these models has been thoroughly considered [6–11, 13–17]. The picture that emerges suggests that collider and direct searches enjoy a high degree of complementarity, with colliders particularly shining for low mass dark matter and for interactions leading to predominantly spin-dependent elastic scattering, and direct searches providing stronger limits for interactions leading to spin-independent scattering and for cases where the collider energies can resolve a light color-singlet mediator [7, 18–21]. Some of the most important connections to indirect detection signals have also been explored [22–30], and indicate that indirect detection is also a very important part of the program of covering the space of allowed interactions. Here, our focus will be primarily on the correlations between the annihilation cross section (with particular interest in inferring the relic density) and the collider production cross section.

### A. Leading Versus Sub-leading Interactions

In some sense, crossing symmetry is a “built-in” component of effective theories where the only interactions of dark matter with Standard Model fields is via local operators. However, a given UV complete theory is likely to populate more than one operator with similarly-sized coefficients, and (as discussed in detail below), there is no guarantee that the same operator will dominate for all three processes. It is well-known that the relativistic behavior of dark matter bilinears is most easily organized by the parity of the bilinear. However, Lorentz and gauge-invariant Lagrangians are naturally built out of Weyl spinors leading to interactions organized in terms of left or right-chiral projections containing both parity-even and parity-odd terms. Thus, it is likely that a term which is leading for direct detection will be accompanied by a related term which will lead for non-relativistic annihilation. Comparing annihilation rates and colliders is more subtle, because the mono-object signal produces dark matter particles relativistically and thus produces dark matter somewhat agnostically with respect to the underlying Lorentz structure. In a typical case, one could easily expect that a single operator will dominate annihilation, but comes with chiral-related terms that contribute at colliders, leading to an order one mismatch between the two descriptions even when the EFT is a good description.

### B. Suppressed Annihilations

We note that at tree level, annihilations of any Majorana fermion dark matter into Standard Model fermions are suppressed. This is a well-known result, and commonly referred to as  $p$ -wave suppression. It is worth mentioning, however, that the annihilation is only strictly  $p$ -wave for interactions which are scalar or axial-vector in nature<sup>2</sup>. In particular, a pseudoscalar-type interaction is allowed, and is suppressed by SM chirality, yet gives rise to  $s$ -wave annihilations. This distinction may seem to be purely academic, but when considering the predictions for indirect dark matter searches versus those for collider production the difference in mechanism of the suppression becomes very important. Chirality suppression is energy-independent, but it does depend on the mass of the SM fermion involved in the process. This means that dark matter sufficiently heavy to annihilate into top quarks is only very weakly suppressed, while attempting to produce dark matter from the light quarks which are prevalent in the

---

<sup>1</sup> The dark matter could be Dirac or Majorana, with the key difference between the two being that certain bi-linears (e.g. the vector and tensor), from which contact interactions with Standard Model fields can be constructed, identically vanish in the Majorana case.

<sup>2</sup> The  $p$ -wave nature of the annihilations of fermions through scalar and axial-vector operators is simple enough to understand intuitively; left- and right-handed fields are indistinguishable at zero velocity, so something which couples to those states with opposite strength will give no contribution in that limit. Scalars and axial vectors do precisely this.

TABLE I: Common operators and their suppression mechanisms with regard to non-relativistic annihilation.

Operator	Suppressed by Chirality	$p$ -wave Suppressed
$\bar{\chi}\chi\bar{q}q$	Yes	Yes
$\bar{\chi}\gamma^5\chi\bar{q}\gamma^5q$	Yes	No
$\bar{\chi}\gamma^\mu\chi\bar{q}\gamma_\mu q$	No	No
$\bar{\chi}\gamma^\mu\gamma^5\chi\bar{q}\gamma_\mu\gamma^5q$	No	Yes
$\bar{\chi}\sigma^{\mu\nu}\chi\bar{q}\sigma_{\mu\nu}q$	Yes	No

proton is very highly suppressed.  $p$ -wave suppression, on the other hand, is directly connected to the low velocity of annihilating WIMPs in the halo, a concern which is totally alleviated when WIMP pairs are produced relativistically at the LHC. If we consider instead a Dirac dark matter candidate, two new types of interactions are allowed. Tensor-type interactions are also suppressed by SM chirality, but are once again allowed to proceed in the  $s$ -wave, while vector-type interactions are not suppressed by anything but the scale of the interaction itself.

Even once we ‘know’ the dark matter spin and remaining within the simple framework of the EFT, what we assume about an observed signal has significant effects on our extrapolation to other experiments. Depending on the Lorentz structure of the operator, dark matter annihilation processes can be unsuppressed,  $p$ -wave suppressed, suppressed by quark masses in accordance with the conjecture of MFV, or suppressed by both of the above. Operators which are suppressed by SM chirality will cause dark matter to annihilate more readily than be produced at colliders (assuming it is heavy enough to annihilate into quarks which are rare in the proton), while operators which allow only  $p$ -wave interactions are more easily probed at colliders than in annihilations. When both of these suppressions are present, the  $p$ -wave suppression is generally more important for the suppression scales which are accessible to experiment (and which can lead to an appropriate relic density), so that collider searches would be the more promising search, but neither search has much reach. We have listed the most commonly considered operators in table I and indicated which suppressions, if any, are present for those operators. The table reveals that this space of operators covers all combinations of suppression, ranging from the vector operator which is completely unsuppressed to the scalar interaction which is both  $p$ -wave *and* chirally-suppressed.

As a particular example, it is instructive to compare the pseudo-scalar and axial vector operators:

$$\bar{\chi}\gamma_5\chi\bar{q}\gamma_5q \quad \text{versus} \quad \bar{\chi}\gamma^\mu\gamma_5\chi\bar{q}\gamma_\mu\gamma_5q. \quad (1)$$

The first is quark-mass suppressed and thus difficult to see at the LHC, while the second is  $p$ -wave suppressed in annihilations. If we had e.g. some signal from collider searches of missing energy production, we could attempt to extrapolate using either of these operators to predict what cross section should be seen in indirect detection. On the one hand, the mass-suppressed operator results in a difference of sea quark versus valence quark parton distribution functions in matching the collider signal, leading to an increase in the necessary interaction strength to produce a given collider result relative to an unsuppressed operator, and ultimately a larger annihilation cross section into heavy quarks. On the other hand, the  $p$ -wave operator picks up a large  $v^2$  suppression for annihilations in the galactic halo. As a result, in this case we estimate that the translation of collider observation to annihilation cross section would differ by more than eight orders of magnitude between these two operators. Of course, ultimately this haziness can be understood as a blessing – if one expected to be sensitive in an indirect search, failing to observe the signal would strongly suggest the axial-vector operator as the origin of the collider observation. Further information could be provided by direct detection experiments, since the pseudo-scalar operator is velocity-suppressed in direct detection, whereas the axial-vector interaction would lead to a spin-dependent signal.

### III. TRICKY SUPERSYMMETRIC THERMAL RELICS

Crossing symmetry can also be subtle in UV complete models of dark matter. Here we focus on the concrete case of the Minimal Supersymmetric Standard Model (MSSM). We intend to provide examples where:

Model	$M_1$	$\mu$	$m_{\tilde{\tau}_1}$	$m_A$	$m_{\chi_1^0}$	$m_h$
Model 1	200	239	8000	1000	182	127
Model 2	194	220	8000	1000	172	128.6
Model 3	200	1000	201	1000	199	130
Model 4	200	1000	8000	454	199	127
Model 5	200	1000	8000	391.5	199	125

TABLE II: Selected input and output parameters (in GeV) for the five supersymmetric benchmark models; see the text for additional details.

- (i) the guideline of having a thermal relic density matching the observed dark matter density fails at making unique predictions for indirect dark matter detection rates, and
- (ii) where predictions for collider rates are wildly different, even if the dark matter is a good thermal relic, and even if dark matter indirect detection rates are comparable and the dark matter particle mass is identical.

All of the models we select have a neutralino as the lightest supersymmetric particle, and feature a thermal relic neutralino density which saturates the observed cosmological dark matter density today. We select points which have particular indirect dark matter detection phenomenologies connected with the various possible dominant mechanisms of dark matter annihilation, in the early and in the late universe. Our points are chosen to illustrate certain cases; for examples of more complete exploration of dark matter in the MSSM, see [4, 31–33].

For all models, we take the ratio of the neutral Higgses vacuum expectation values,  $\tan\beta = 15$ , and, unless otherwise specified, we take  $m_A = 1$  TeV,  $M_2 = M_3 = 1$  TeV,  $M_1 = 200$  GeV, all tri-scalar couplings are set to zero and, again unless otherwise specified (for Model 3), we take the scalar soft supersymmetry-breaking sfermion masses to be 8 TeV. The model parameters quoted in Tab. II are all tuned to produce the observed dark matter abundance in the form of thermal relic neutralinos. In addition, in all models the Higgs mass is compatible with recent results from the LHC collaborations within the experimental and theoretical uncertainties. Tab. II collects the relevant input parameters, as well as the output lightest neutralino mass  $m_{\chi_1^0}$  and the lightest CP-even neutral Higgs  $m_h$ . All masses and mass parameters are given in GeV in the table.

In Models 1 and 2, the thermal relic density is set by the lightest neutralino having a sizable higgsino fraction, and by coannihilation with the lightest chargino and the next-to-lightest neutralino. This is achieved by tuning the higgsino mass parameter  $\mu$  to values close to the bino soft supersymmetry breaking mass term  $M_1$ . The difference between our “benchmark” Model 1 and Model 2 is that in the latter case the lightest neutralino mass was tuned to be slightly below the top quark mass threshold. In the early universe, and specifically at thermal freeze-out, when  $T \simeq m_{\chi_1^0}/20 \approx 8.5$  GeV, pair-annihilation into top quarks was kinematically accessible for large enough neutralino velocities, while in the late universe the top annihilation channel is entirely closed. This provides an example of how the relevant pair annihilation cross section in the early versus late universe can differ. Note that for our particular parameter space choice, the effect is not particularly dramatic, namely reducing the pair annihilation cross section today by approximately a factor of 2 with respect to the early universe (see Tab. IV). This is due to the fact that for both Models 1 and 2 the pair-annihilation into  $W^+W^-$  or  $ZZ$  final states is relatively important, on the same order as the pair-annihilation into top quark pairs.

Model 3 is an instance of a model where the thermal relic density is set by the co-annihilation with the lightest stau, whose mass was fine-tuned to be approximately 1 GeV above the lightest neutralino mass. In this case, the neutralino pair annihilation cross section is highly suppressed (in fact,  $\langle\sigma v\rangle \sim 10^{-28}$  cm<sup>3</sup>/s) as the effective cross section setting the thermal relic density is dominated by stau annihilation (45%) and co-annihilation (50%).

Models 4 and 5 feature a Higgs particle with a mass close to twice the lightest neutralino mass, thus opening a resonant pair-annihilation  $s$ -channel where the lightest neutralino annihilates via a close-to-on-shell scalar into (typically) fermion-antifermion final states. In Model 4, the lightest neutralino mass is

Model	Total EW $\sigma$ (fb)	$\chi_1^0\chi_1^0$ $\sigma$ (fb)	Inclusive $\chi\chi$ $\sigma$ (fb)	$\tilde{\tau}^+\tilde{\tau}^-$ $\sigma$ (fb)
Model 1	625	0.2	625	0
Model 2	850	0.3	850	0
Model 3	9.9	0.001	2.8	7.1
Model 4	2.8	0.001	2.8	0
Model 5	2.8	0.001	2.8	0

TABLE III: LHC pair-production cross sections for the stated electroweakly-charged particles in each of the five benchmark models

below the  $m_A/2$  threshold, while for Model 5 we tune  $m_A$  so that  $m_\chi > m_A/2$ . In both cases the late-time cross section is off-resonance. However, due to finite-temperature effects, the late-time annihilation rate is larger than the naive expectation (from  $s$ -wave annihilation) for Model 5, while it’s smaller for Model 4, as we explain below.

The late-universe (i.e.  $T = 0$ ) pair-annihilation cross section for Model 4 is *smaller* than the reference thermal cross section ( $3 \times 10^{-26}$  cm<sup>-3</sup>/s) at a value of  $6.4 \times 10^{-27}$  cm<sup>-3</sup>/s: the early-universe finite-temperature cross section, responsible for setting the thermal relic density, results from the convolution of a temperature kernel times the cross section, which at  $\sqrt{s} > 2m_\chi$  is increasingly more “on-resonance”. Vice versa, for Model 5 the resonance is increasingly off shell in the early universe, while it’s closer to being on shell in the late universe, resulting in a pair-annihilation cross section today larger than the naive thermal  $s$ -wave prediction, at  $5.2 \times 10^{-26}$  cm<sup>-3</sup>/s.

In what follows we outline predictions for collider searches (sec. III A) and for indirect detection searches (sec. III B) for the five benchmark models outlined above, and show that even within the restrictive framework of the MSSM, models with the same neutralino mass and with the correct thermal neutralino relic abundance produce a very broad set of outcomes for “cross-symmetric” processes.

### A. Collider Predictions

For each of the benchmark models described above, we calculate the pair production cross section for supersymmetric particles. The total production cross sections as well as a breakdown into subprocesses of particular interest, including direct production of pairs of LSPs ( $\chi_1^0$ ), the sum of all pairs of neutralinos and/or charginos (Inclusive  $\chi\chi$ ), and pairs of lightest staus ( $\tilde{\tau}_1^+\tilde{\tau}_1^-$ ) are shown in Table III. Note that outside of Model 3, the stau pair production cross section vanishes since  $m_{\tilde{\tau}_1}$  is set to 8 TeV, as indicated in table II. The heavier  $\tilde{\tau}$  is always chosen to have a mass of 8 TeV. As all of the colored particles have been chosen to be heavy enough to be decoupled, electroweak production mechanisms are dominant. The usual jets and missing energy search corresponds to pair production of the lightest neutralino with an additional hard initial state radiation (ISR) jet, and therefore is bounded from above by the  $\chi_1^0$  pair production cross section. Note that in all of the models we consider here, this cross section is smaller than a femtobarn.

Even in our “vanilla” benchmark Model 1, where the neutralino is well-tempered and mixing is the factor which drives the relic density, direct dark matter production at the LHC is very small. While these models do respect crossing symmetry well, by construction, annihilations do not proceed dominantly to quark final states, and thus a production cross section comparable to the annihilation cross section cannot be achieved by a hadron collider. This illustrates a first crossing symmetry issue: collider searches are sensitive to having very selected final states in the cross-symmetric annihilation process, and such final states are not generic. A “weak boson collider” would best probe the physics which leads to the dark matter relic density in these situations. Model 2, featuring the sub-top quark mass threshold, also exhibits similar behaviour (since the top threshold does not impact the collider production cross section).

We also see strong suppression of SUSY production cross sections when the dominant contributor to the effective pair-annihilation cross section in the early universe is coannihilation, in our case with staus. This allows the dark matter to be much more weakly coupled to standard matter than naively expected

Model	$\langle\sigma v\rangle_0$	$\langle\sigma v\rangle_{\gamma\gamma}/\langle\sigma v\rangle_0$	$\phi_\gamma(E > 1 \text{ GeV})$	$\phi_{\gamma\gamma}$	$\sigma_{\chi P}^{\text{SI}}$	$\sigma_{\chi P}^{\text{SD}}$
Model 1	$2.03 \times 10^{-26}$	$3.50 \times 10^{-5}$	$1.73 \times 10^{-9}$	$6.50 \times 10^{-15}$	$1.62 \times 10^{-8}$	$1.53 \times 10^{-4}$
Model 2	$1.37 \times 10^{-26}$	$1.32 \times 10^{-4}$	$1.26 \times 10^{-9}$	$2.31 \times 10^{-14}$	$1.81 \times 10^{-8}$	$2.01 \times 10^{-4}$
Model 3	$9.20 \times 10^{-29}$	$8.99 \times 10^{-3}$	$1.91 \times 10^{-12}$	$4.44 \times 10^{-15}$	$5.38 \times 10^{-11}$	$1.34 \times 10^{-7}$
Model 4	$6.39 \times 10^{-27}$	$1.55 \times 10^{-8}$	$2.92 \times 10^{-10}$	$5.69 \times 10^{-19}$	$2.50 \times 10^{-10}$	$1.34 \times 10^{-7}$
Model 5	$5.18 \times 10^{-26}$	$9.19 \times 10^{-7}$	$2.86 \times 10^{-9}$	$2.73 \times 10^{-16}$	$3.97 \times 10^{-10}$	$1.23 \times 10^{-7}$

TABLE IV: Dark matter detection results for the five supersymmetric benchmark models; the first column indicates the zero-temperature thermally averaged pair-annihilation cross section times velocity, in units of  $\text{cm}^3/\text{s}$ ; the second column gives the branching ratio for annihilation into two photons; the third column indicates the integrated photon flux above 1 GeV from the direction of the Galactic center, in  $\text{cm}^{-2}\text{s}^{-1}$ , and the fourth column the  $\gamma\gamma$  flux, in the same units. Lastly, columns 6 and 7 indicate the neutralino- proton scattering cross section, respectively spin-independent and spin-dependent, in units of pb.

from crossing symmetry arguments, while still generating the correct relic density, further divorcing the model from the expectation of a comparable production cross section. In this case a tau collider, while perhaps unlikely to be realized in the foreseeable future, would be the optimal choice to produce dark matter pairs while probing the physics which leads to the relic density.

Models 4 and 5 feature an  $A^-$  (and  $H^-$ ) funnel to get the correct relic density of dark matter, and thus have very little production cross section of any SUSY particles at all at the LHC, as those states couple very weakly to light quarks. In this case, the best probe of dark matter phenomena is contained within Higgs physics, where the heavier state can be produced and its couplings measured. However, even with the discovery of new heavy scalars, additional complications can arise. As discussed above, the distinction between Models 4 and 5 is that in one case the dark matter is just lighter than  $M_A/2$ , and in the other just heavier. In the second case the invisible width will actually vanish, and no notable sign of dark matter will be present in on-shell Higgs processes. It is only with an independent dark matter mass measurement that the funnel origin of the relic abundance in this model can be divined.

## B. Indirect Detection Predictions

In this section we compare predictions for indirect detection rates for the 5 benchmark “tricky” thermal neutralinos described above. We collect the relevant detection rates in tables IV and V. In addition to the thermally averaged pair-annihilation cross section, listed in the second column, table IV lists the branching ratio into the two-photon final state in column 3. Interestingly, the largest branching ratio corresponds to Model 3, i.e. the model with very light staus where stau coannihilation drives the thermal relic density. In this case, in fact, the relevant loop process includes the light staus, and, as can be seen from the second column, the total neutralino pair-annihilation cross section is quite suppressed, resulting in a relatively large (almost per-cent level)  $\langle\sigma v\rangle_{\gamma\gamma}/\langle\sigma v\rangle_0$  branching ratio. We show relevant differential spectra (times particle energy squared) in Figure 1: the top-left panel shows our predictions for gamma rays, the top right for antiprotons, the bottom left for positrons and, finally, the bottom right for neutrinos from the Sun. The difference between Models 4 and 5 are ascribed to the different  $T = 0$  pair-annihilation cross sections, as discussed above. The one exception is the flux of neutrinos from the Sun, which is dominated by the capture rate (similar for the two models) rather than by the annihilation rate, due to capture-annihilation equilibrium.

We calculate the integrated gamma-ray flux from from within a  $10^{-3}$  sr solid angle of the direction of the Galactic center and for energies above 1 GeV in column 4. We assume a smooth Navarro-Frenk-White dark matter density profile [34], with a local halo density of  $0.3 \text{ GeV}/\text{cm}^3$ , a heliocentric distance of 8 kpc, and a scale radius of 20 kpc. Our results are relatively homogeneous for Models 1, 2, 4 and 5, all at the level of  $10^{-9} \text{ cm}^{-2}\text{s}^{-1}$ , with mild differences due to slightly different  $\gamma$ -ray spectra (see the top-left panel of Figure 1) and to the slightly differing pair-annihilation cross sections (column 2). The markedly different flux prediction, and the strikingly different spectrum shown in the figure, are due to

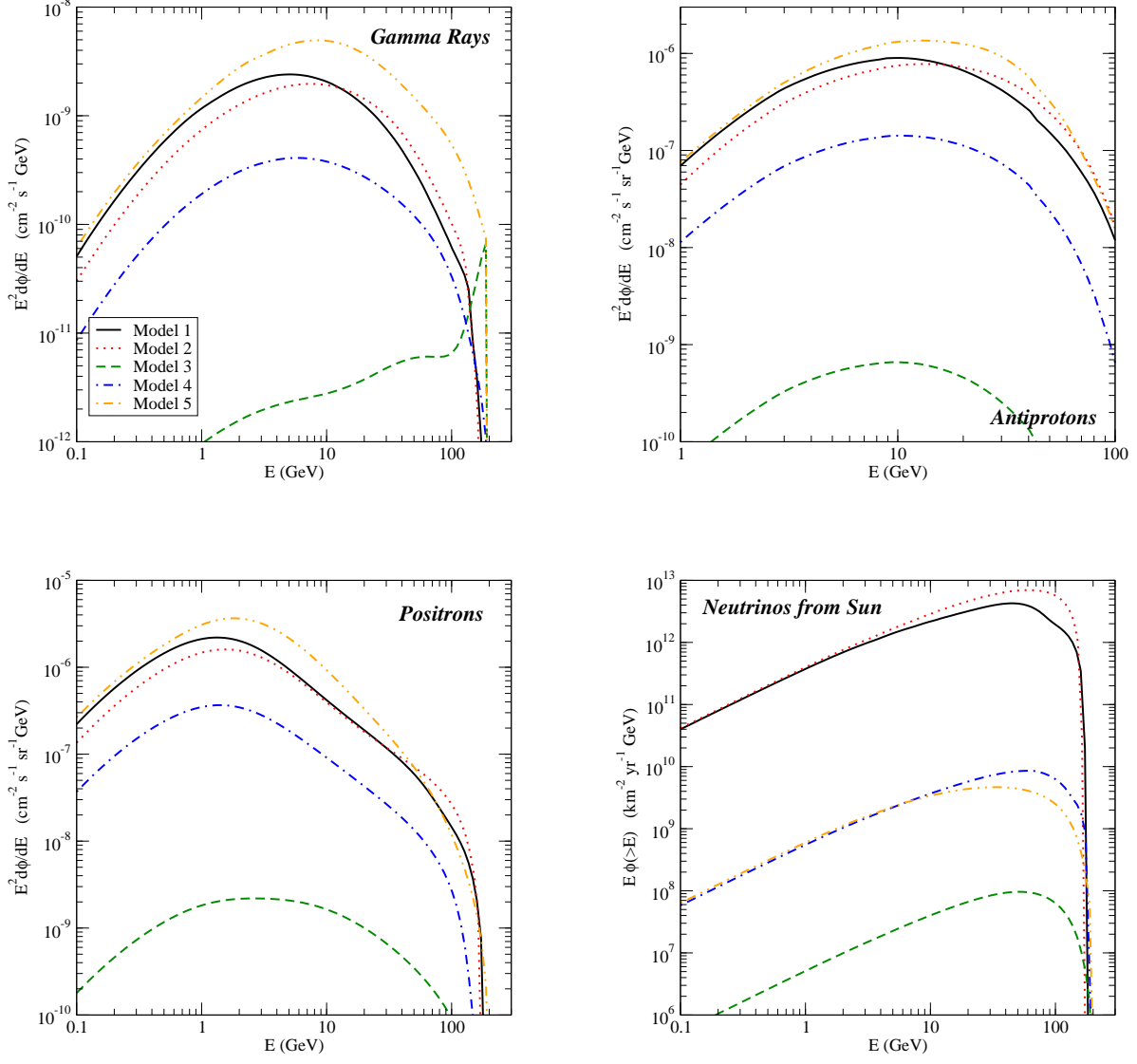


FIG. 1: Differential particle spectra times energy squared for our five “tricky thermal neutralinos” benchmark models, for gamma rays (top left panel), antiprotons (top right), positrons (bottom left) and neutrinos from the Sun (bottom right). Particle energies are in GeV, while spectra are in units of  $\text{GeV}^{-2} \text{cm}^{-2} \text{s}^{-1} \text{sr}^{-1}$ .  $\text{sr}^{-1}$ , with the exception of neutrinos, for which we use  $\text{GeV}^{-2} \text{km}^{-2} \text{yr}^{-1}$ .

the dominant  $\tau^+\tau^-$  final state, dictated by the Model’s particle spectrum, which features light staus as the only relevant mediators for the annihilation process.

Column 5 lists, for the same astrophysical setup as column 4, the predicted monochromatic  $\gamma\gamma$  flux. In this case we uniformly get suppressed rates, but with larger differences, due to different lightest neutralino compositions for Models 1 and 2 and to the different Higgs boson masses for Models 4 and 5, with Model 3 featuring a relatively large flux (especially compared to the continuum flux of column 4) due to light



Model	$\phi_{\mu}^{\oplus}(E > 1 \text{ GeV})$	$\phi_{\mu}^{\ominus}(E > 1 \text{ GeV})$	$\phi_{\mu}^{\oplus}(E > 100 \text{ GeV})$	$\phi_{\mu}^{\ominus}(E > 100 \text{ GeV})$	$\phi_{\bar{p}}$	$\phi_{e^+}$	$\phi_{\bar{D}}$
Model 1	$1.023 \times 10^{-3}$	462.	$5.31 \times 10^{-5}$	17.7	$8.98 \times 10^{-9}$	$2.11 \times 10^{-6}$	$1.61 \times 10^{-12}$
Model 2	$1.88 \times 10^{-3}$	896.	$1.09 \times 10^{-4}$	41.9	$7.49 \times 10^{-9}$	$1.47 \times 10^{-6}$	$6.21 \times 10^{-13}$
Model 3	$2.93 \times 10^{-11}$	0.013	$9.97 \times 10^{-13}$	$5.68 \times 10^{-4}$	$6.60 \times 10^{-12}$	$1.82 \times 10^{-9}$	$1.42 \times 10^{-15}$
Model 4	$3.35 \times 10^{-8}$	1.11	$6.85 \times 10^{-10}$	0.070	$1.42 \times 10^{-9}$	$3.48 \times 10^{-7}$	$2.02 \times 10^{-13}$
Model 5	$2.91 \times 10^{-7}$	0.553	$5.88 \times 10^{-9}$	0.0221	$1.32 \times 10^{-8}$	$3.07 \times 10^{-6}$	$1.29 \times 10^{-12}$

TABLE V: More Indirect detection results for the five supersymmetric benchmark models: columns 2 and 3 indicate the integrated muon flux above 1 GeV from the Earth and from the Sun, respectively, in units of  $\text{km}^{-2}\text{yr}^{-1}$ ; columns 4 and 5 show the same quantity, but integrated above 100 GeV. The last three columns indicate the differential antiproton flux at 10 GeV (col. 6), positron flux at 1 GeV (col. 7) and antideuteron flux at 1 GeV (col. 8) all in units of  $\text{GeV}^{-1} \text{cm}^{-2} \text{s}^{-1} \text{sr}^{-1}$ .

staus running in the loop diagrams.

The last two columns indicate the direct detection cross sections for elastic neutralino-proton interactions, for spin-independent (col. 6) and spin-dependent (col. 7) processes. We note the large differences among the 5 benchmark models for both  $\sigma_{\chi p}^{\text{SI}}$  and  $\sigma_{\chi p}^{\text{SD}}$ . These are due to markedly different higgsino fractions, which are relatively large for Models 1 and 2 and very small for models 3, 4 and 5. The relatively small differences between models 4 and 5 are due to the different heavy Higgs boson masses. This set of models thus also stands as an example of how models with the same neutralino mass and comparable pair annihilation cross sections can have drastically different (here at the level of 3 orders of magnitude) direct detection cross sections.

We continue our survey of indirect detection rates in table V, which lists the flux of muons from the Earth or the Sun produced by neutrinos generated by dark matter annihilation. We show the integrated flux above 1 GeV (columns 2 and 3) since experimental limits are often given utilizing this threshold, and the physically more relevant 100 GeV threshold (columns 4 and 5), which gives a more realistic idea of the expected event rate in a telescope similar to, for example, IceCube. Fluxes are quoted in units of  $\text{km}^{-2}\text{yr}^{-1}$ .

The driver for the flux of muons from the Earth and from the Sun is the capture rate, which, in turn, depends on the scattering cross section of neutralinos off of nuclei. It is therefore not surprising that we find a hierarchy between Models 1 and 2 versus models 4 and 5 that reproduces the hierarchy observed in the last two columns of table IV. The slightly softer high-energy neutrino spectrum for Model 5 (see fig. 1) explains the additional suppression for the  $> 100 \text{ GeV}$  flux for Model 5 versus Model 4. In the case of Model 3, equilibration between capture and annihilation does not occur due to the low pair-annihilation cross section, and the rates are further suppressed.

The last three columns of table V indicate the differential antiproton flux at 10 GeV (col. 6), positron flux at 1 GeV (col. 7) and antideuteron flux at 1 GeV (col. 8) all in units of  $\text{GeV}^{-1} \text{cm}^{-2} \text{s}^{-1} \text{sr}^{-1}$ . The rates are generically consistent with the pair-annihilation cross section levels quoted in table IV. The spectra we find are relatively comparable, with harder spectra found for Model 2 and especially 4, due to the relatively large pair-annihilation rate into  $\tau^+\tau^-$  pairs (which is suppressed compared to the  $b\bar{b}$  final states by factors of the mass ratio squared and of color). As a side note, we find that the positron spectra are in all cases too soft to reproduce the positron fraction anomaly reported by AMS-02 [35].

#### IV. CATASTROPHIC FAILURES OF CROSSING SYMMETRY

In this section we provide two examples of dark matter models that have received considerable attention in the recent past, and where arguments based on crossing symmetry to predict indirect detection and collider rates badly fail: models with a so-called Sommerfeld effect (sec. IV A) and inelastic dark matter models (sec. IV B).

### A. Very Light Mediators and Sommerfeld-like Enhancement

In a model where dark matter can self-interact by the exchange of very light mediators, the non-relativistic cross section can receive a large Sommerfeld-like enhancement for dark matter scattering at low relative velocity. This already implies a large velocity dependence of the cross section leading to a much larger annihilation rate for WIMPs in the Galaxy (whose velocity dispersion is thought to be order  $10^{-3}$ ) compared to freeze-out, when  $v \sim 10^{-1}$ .

The mapping between annihilation and colliders may also be convoluted by the presence of the light mediator. At colliders, dark matter is only visible when produced relativistically, and a mediator leading to self-scattering is largely irrelevant for the typical missing energy signals. Furthermore, annihilation may have a large component into the mediator particles themselves, and this rate is generically difficult to infer from the usual collider searches for dark matter. While it may be possible to produce the dark mediator at colliders (for example, radiated from a final state WIMP in a process which otherwise produces dark matter), the signature of the mediator is very model-dependent, with some mediators decaying very quickly to SM states (see e.g. [36] for a discussion of a specific model), and others stable on collider scales and thus at most appearing as a slight discrepancy in the distribution of missing momentum [37].

We note that large Sommerfeld-like enhancements are correlated with the presence of light mediators, for which colliders may see non-negligible effects from dark matter bound states, or WIMPonia [38]. Such particles appear as resonances in SM scattering, and thus imply a new type of signal which can be associated with the presence of the enhanced annihilation cross section. The bound state spectra and effective coupling to the SM are very sensitive to the masses of both the dark matter and the mediator, as well as the dark matter-mediator coupling. Detailed measurements of both the bound states and the coupling of unbound WIMPs to SM fields could potentially be combined to infer the presence of Sommerfeld-like enhancements in annihilation.

### B. Inelastic Dark Matter

Inelasticity completely removes the crossing symmetry between collider production and annihilation, since the collider can produce one dark matter particle and one excited state, while annihilation will have to proceed through a  $t$ -channel excited state. Dedicated studies of collider sensitivity to dark matter inelasticity have been performed [39], but they find sensitivity only for splittings much larger than those required for the inelastic scattering phenomenon in direct detection which originally motivated these models. For smaller splittings the excited dark matter state is effectively collider stable, and thus inelastic models cannot generally be distinguished from ordinary dark matter at colliders.

The long lifetime of the excited state often leads to the dark matter relic density being set, not by WIMP-WIMP annihilations, but rather by WIMP-excited state coannihilations, so that the crossing symmetry between colliders and annihilations setting the relic density may actually remain largely intact. However, at late cosmological times the excited states in many models will have largely decayed down to WIMPs and soft photons or neutrinos, such that the annihilations we are currently searching for are no longer the same as those which set the relic density.

In the case of one particular model with excited dark matter states the symmetry is broken even more completely. For Exciting Dark Matter [40] indirect detection has already seen indications of dark matter's physics in the INTEGRAL 511 keV excess, but this is not in fact an indication of annihilation at all. Rather, the excess is due entirely to the decays of the excited states back down to the WIMP ground state. Depending on parameter choices the excited state could still be collider stable or it could decay promptly to a soft electron-positron pair and a WIMP. Distinguishing between these two cases would be challenging at the LHC, where soft leptons are useless as triggers and difficult to identify.

The final member of the class of inelastically scattering dark matter models scatter exothermically [41]. Such models have recently been invoked [42] to reconcile a dark matter interpretation of the excess CDMS silicon events [43] with the stringent bounds from Xenon experiments [44] (for alternative explanations, see [45, 46]). In this case it is the excited dark state which is the initial state in observable scattering events, which necessitates that the excited state have a cosmological lifetime, something not required in other inelastic models. With this assumption, a large fraction of the galactic halo can be

TABLE VI: Candidate models for Exothermic Dark Matter in CDMS Si

Operator	$\Lambda$ (GeV)	$\sigma(pp \rightarrow \chi_1\chi_2)$ (fb)	$\sigma(\chi_1\chi_2 \rightarrow \bar{q}q) * v$ (cm <sup>3</sup> /s)
$\bar{\chi}_1\chi_2 \bar{q}q$	260	5.3	$4.88 \times 10^{-37}$
$\bar{\chi}_1\gamma_\mu\chi_2 \bar{q}\gamma^\mu q$	13570	0.44	$3.9 \times 10^{-32}$

composed of the excited states. Interestingly, in this case the annihilation does look like a crossing of the scattering process, as there are plenty of both states of dark matter available to find each other and annihilate. Likewise colliders remain insensitive to the splitting between the two dark states and bound the interaction strength without regard to the exothermic phenomenology. Thus, it seems that crossing symmetry between colliders and annihilations remains robust, while the relation with direct detection is the only case which is altered.

Indeed, manifest crossing symmetry as described in section II is present between the indirect and collider searches for dark matter, but we find ourselves with precisely the same potential for confusion between operators as were described there. There are two candidate operators that could generate appreciable exothermic scattering of dark matter on nuclei,

$$\sum_q \frac{m_q}{\Lambda^3} \bar{\chi}_1\chi_2 \bar{q}q + \text{h.c.} \quad (2)$$

$$\sum_q \frac{1}{\Lambda^2} \bar{\chi}_1\gamma_\mu\chi_2 \bar{q}\gamma^\mu q + \text{h.c.} \quad (3)$$

with other choices suppressed by the mass splitting of the dark matter states and/or the small typical velocities of WIMPs in the galactic halo. As previously discussed, the former is chirality-suppressed while the latter is unsuppressed, and thus these lead to very different phenomenologies for annihilations as compared to pair production at colliders. We consider a specific representative point from [42], choosing a dark matter mass of 5 GeV and a WIMP-nucleon scattering cross section of  $3 \times 10^{-43}$  cm<sup>2</sup>. The suppression scales needed to induce this scattering rate, as well as the pair production cross section at the 14 TeV LHC and the pair annihilation cross section corresponding to that suppression scale are presented in table VI. We point out that these are both equally good fits to the CDMS Si events, and yet the choice of operators leads to differences of one order of magnitude in collider signal strength and five orders of magnitude in indirect detection, with the effects running in opposite directions. This is a concrete example of the effects considered in section II that is of particular current interest.

## V. CONCLUSIONS

There is excellent reason to think that we stand at the brink of important discoveries related to dark matter. Once these begin, the primary task for particle physics will be to assimilate the message into a successor theory to the Standard Model which includes dark matter, and then to use that theory to firmly establish a cosmological picture explaining its relic density. As we assemble information from direct detection, indirect detection, and colliders, crossing interactions will play a decisive role.

In this article we have explored several different visions of dark matter, ranging from sketches of interactions based on effective field theories to UV-complete models such as the MSSM. In all cases, we could identify cases where confusion was likely to arise. But rather than representing serious problems in our ability to reconstruct the underlying theory of dark matter from a discovery, the examples we provide instead show the necessity and strength of the multi-pronged search program which is currently underway. In the end, the apparent contradictions arising from simple extrapolations will turn into the tool which will guide us on the path to constructing a theory of dark matter in the context of a new Standard Model for particle physics.

### Acknowledgements

TMPT is grateful to conversations with Tune Kamae. WS and SP are partly supported by the US Department of Energy under contract DE-FG02-04ER41268. The research of TMPT. is supported in part by NSF grant PHY-0970171 and by the University of California, Irvine through a Chancellor's fellowship.

- 
- [1] D. Bauer, J. Buckley, M. Cahill-Rowley, R. Cotta, A. Drlica-Wagner, J. Feng, S. Funk and J. Hewett *et al.*, arXiv:1305.1605 [hep-ph].
  - [2] J. M. Cornell, S. Profumo and W. Shepherd, arXiv:1305.4676 [hep-ph].
  - [3] M. Beltran, D. Hooper, E. W. Kolb, Z. A. C. Krusberg and T. M. P. Tait, JHEP **1009**, 037 (2010) [arXiv:1002.4137 [hep-ph]].
  - [4] M. Cahill-Rowley, R. Cotta, A. Drlica-Wagner, S. Funk, J. Hewett, A. Ismail, T. Rizzo and M. Wood, arXiv:1305.6921 [hep-ph].
  - [5] G. Bertone, K. Kong, R. R. de Austri and R. Trotta, Phys. Rev. D **83**, 036008 (2011) [arXiv:1010.2023 [hep-ph]].
  - [6] J. Goodman, M. Ibe, A. Rajaraman, W. Shepherd, T. M. P. Tait and H. -B. Yu, Phys. Lett. B **695**, 185 (2011) [arXiv:1005.1286 [hep-ph]].
  - [7] Y. Bai, P. J. Fox and R. Harnik, JHEP **1012**, 048 (2010) [arXiv:1005.3797 [hep-ph]].
  - [8] J. Goodman, M. Ibe, A. Rajaraman, W. Shepherd, T. M. P. Tait and H. -B. Yu, Phys. Rev. D **82**, 116010 (2010) [arXiv:1008.1783 [hep-ph]].
  - [9] A. Rajaraman, W. Shepherd, T. M. P. Tait and A. M. Wijangco, Phys. Rev. D **84**, 095013 (2011) [arXiv:1108.1196 [hep-ph]].
  - [10] P. J. Fox, R. Harnik, J. Kopp and Y. Tsai, Phys. Rev. D **85**, 056011 (2012) [arXiv:1109.4398 [hep-ph]].
  - [11] P. J. Fox, R. Harnik, R. Primulando and C. -T. Yu, Phys. Rev. D **86**, 015010 (2012) [arXiv:1203.1662 [hep-ph]].
  - [12] G. D'Ambrosio, G. F. Giudice, G. Isidori and A. Strumia, Nucl. Phys. B **645**, 155 (2002) [hep-ph/0207036].
  - [13] U. Haisch and F. Kahlhoefer, JCAP **1304**, 050 (2013) [arXiv:1302.4454 [hep-ph]].
  - [14] U. Haisch, F. Kahlhoefer and J. Unwin, arXiv:1208.4605 [hep-ph].
  - [15] P. J. Fox and C. Williams, Phys. Rev. D **87**, 054030 (2013) [arXiv:1211.6390 [hep-ph]].
  - [16] T. Lin, E. W. Kolb and L. -T. Wang, arXiv:1303.6638 [hep-ph].
  - [17] H. Dreiner, D. Schmeier and J. Tattersall, Europhys. Lett. **102**, 51001 (2013) [arXiv:1303.3348 [hep-ph]].
  - [18] J. Goodman, W. Shepherd, [arXiv:1111.2359 [hep-ph]].
  - [19] I. M. Shoemaker and L. Vecchi, Phys. Rev. D **86**, 015023 (2012) [arXiv:1112.5457 [hep-ph]].
  - [20] H. An, X. Ji and L. -T. Wang, JHEP **1207**, 182 (2012) [arXiv:1202.2894 [hep-ph]].
  - [21] M. T. Frandsen, F. Kahlhoefer, A. Preston, S. Sarkar and K. Schmidt-Hoberg, JHEP **1207**, 123 (2012) [arXiv:1204.3839 [hep-ph]].
  - [22] M. Beltran, D. Hooper, E. W. Kolb and Z. C. Krusberg, Phys. Rev. D **80**, 043509 (2009) [arXiv:0808.3384 [hep-ph]].
  - [23] Q. -H. Cao, C. -R. Chen, C. S. Li and H. Zhang, JHEP **1108**, 018 (2011) [arXiv:0912.4511 [hep-ph]].
  - [24] J. Goodman, M. Ibe, A. Rajaraman, W. Shepherd, T. M. P. Tait and H. -B. Yu, Nucl. Phys. B **844**, 55 (2011) [arXiv:1009.0008 [hep-ph]].
  - [25] K. Cheung, P. -Y. Tseng and T. -C. Yuan, JCAP **1101**, 004 (2011) [arXiv:1011.2310 [hep-ph]].
  - [26] K. Cheung, P. -Y. Tseng and T. -C. Yuan, JCAP **1106**, 023 (2011) [arXiv:1104.5329 [hep-ph]].
  - [27] K. Cheung, P. -Y. Tseng, Y. -L. S. Tsai and T. -C. Yuan, JCAP **1205**, 001 (2012) [arXiv:1201.3402 [hep-ph]].
  - [28] A. Rajaraman, T. M. P. Tait and D. Whiteson, JCAP **1209**, 003 (2012) [arXiv:1205.4723 [hep-ph]].
  - [29] M. T. Frandsen, U. Haisch, F. Kahlhoefer, P. Mertsch and K. Schmidt-Hoberg, JCAP **1210**, 033 (2012) [arXiv:1207.3971 [hep-ph]].
  - [30] J. -Y. Chen, E. W. Kolb and L. -T. Wang, arXiv:1305.0021 [hep-ph].
  - [31] R. C. Cotta, K. T. K. Howe, J. L. Hewett and T. G. Rizzo, Phys. Rev. D **85**, 035017 (2012) [arXiv:1105.1199 [hep-ph]].
  - [32] R. C. Cotta, A. Drlica-Wagner, S. Murgia, E. D. Bloom, J. L. Hewett and T. G. Rizzo, JCAP **1204**, 016 (2012) [arXiv:1111.2604 [hep-ph]].
  - [33] M. W. Cahill-Rowley, J. L. Hewett, S. Hoeche, A. Ismail and T. G. Rizzo, Eur. Phys. J. C **72**, 2156 (2012) [arXiv:1206.4321 [hep-ph]].
  - [34] J. F. Navarro, C. S. Frenk and S. D. M. White, Astrophys. J. **490**, 493 (1997) [astro-ph/9611107].

- [35] M. Aguilar *et al.* [AMS Collaboration], Phys. Rev. Lett. **110**, no. 14, 141102 (2013).
- [36] N. Arkani-Hamed and N. Weiner, JHEP **0812**, 104 (2008) [arXiv:0810.0714 [hep-ph]].
- [37] G. F. Giudice, B. Gripaios, R. Mahbubani, [arXiv:1108.1800 [hep-ph]].
- [38] W. Shepherd, T. M. P. Tait and G. Zaharijas, Phys. Rev. D **79**, 055022 (2009) [arXiv:0901.2125 [hep-ph]].
- [39] Y. Bai and T. M. P. Tait, Phys. Lett. B **710**, 335 (2012) [arXiv:1109.4144 [hep-ph]].
- [40] D. P. Finkbeiner and N. Weiner, Phys. Rev. D **76**, 083519 (2007) [astro-ph/0702587].
- [41] P. W. Graham, R. Harnik, S. Rajendran and P. Saraswat, Phys. Rev. D **82**, 063512 (2010) [arXiv:1004.0937 [hep-ph]].
- [42] M. T. Frandsen, F. Kahlhoefer, C. McCabe, S. Sarkar and K. Schmidt-Hoberg, arXiv:1304.6066 [hep-ph].
- [43] R. Agnese *et al.* [CDMS Collaboration], [arXiv:1304.4279 [hep-ex]].
- [44] E. Aprile *et al.* [XENON100 Collaboration], Phys. Rev. Lett. **109**, 181301 (2012) [arXiv:1207.5988 [astro-ph.CO]].
- [45] R. C. Cotta, A. Rajaraman, T. M. P. Tait and A. M. Wijangco, arXiv:1305.6609 [hep-ph].
- [46] J. L. Feng, J. Kumar and D. Sanford, arXiv:1306.2315 [hep-ph].